10MHz, due to the negative feedback mechanism. The high-precision CCII consumes only 3.78mW, indicating the promising potential of the proposed technique.

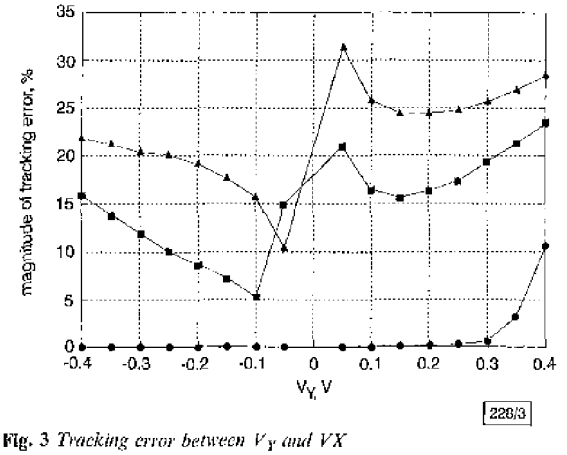

Fig. 3 *Tracking error between V_Y and VX*

R_X = 5kΩ
● proposed CCII
■ SIVF CCII
▲ GIVF CCII

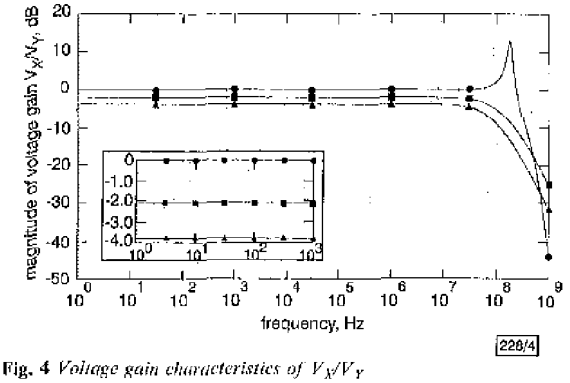

Fig. 4 *Voltage gain characteristics of V_X/V_Y*

R_X = 1kΩ, C_X = 10 pF
● proposed CCII
■ SIVF CCII
▲ GIVF CCII

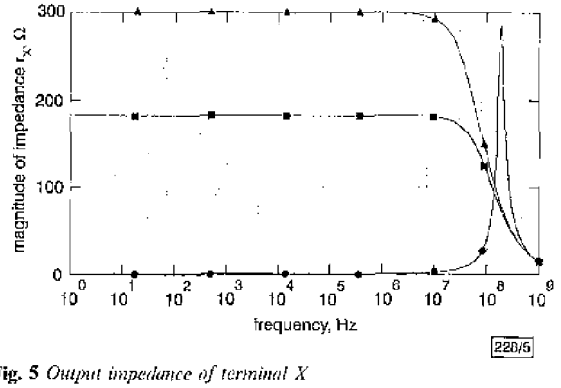

Fig. 5 *Output impedance of terminal X*

C_Y = 10pF
● proposed CCII
■ SIVF CCII
▲ GIVF CCII

Conclusions: Based on the application of local negative feedback to reduce the voltage variations of the nodes affecting voltage transfer accuracy, high precision in voltage tracking and very-low small-signal resistance of the X terminal can be obtained simultaneously. Additionally, high precision in current transfer can be easily accomplished by using high-swing cascode current mirrors. The proposed technique has been effectively applied to the CMOS realisation of a current conveyor in order to enhance the performance to a level comparable to that which can be achieved using BJT versions without the penalty of power consumption.

11 February 2000
Electronics Letters Online No. 20000534
DOI: 10.1049/el:20000534

U. Yodprasit (*Department of Electronic Engineering, Faculty of Engineering, Mahanakorn University of Technology, 51 Cheumsamphan Road, Nong-Chok, Bangkok, Bangkok 10530, Thailand*)

E-mail: uroschanit@mail.ee.mut.ac.th

References

1 SEDRA, A.S., ROBERTS, G.W., and GOHH, F.: 'The current conveyor: history, progress and new results', *IEE Proc. G, Circuits Devices Syst.*, 1990, **137**, (2), pp. 78–87
2 KAULBERG, T.: 'A CMOS current-mode operational amplifier', *IEEE J. Solid-State Circuits*, 1993, **28**, (7), pp. 849–852
3 SACKINGER, E., and GUGGENBUHL, W.: 'A high-swing, high-impedance MOS cascode circuit', *IEEE J. Solid-State Circuits*, 1990, **25**, pp. 289–298

Oscillator circuit configuration for quartz-crystal-resonator sensors subject to heavy acoustic load

V. Ferrari, D. Marioli and A. Taroni

An oscillator circuit configuration is presented to track accurately the resonant frequency and to increase the operating range of quartz-crystal-resonator sensors subject to heavy acoustic loading. The circuit is based on a block for the active cancellation of the crystal electrical capacitance, inserted in a phaselocked loop oscillator. Experimental results confirming the successful application of the principle are reported.

Introduction: The electrical impedance of quartz-crystal-resonator sensors based on AT-cut crystals vibrating in thickness-shear mode (TSR) varies around the crystal resonances when an acoustic load is applied in contact with the sensor surface. Mass microbalances, film-thickness monitors, and gravimetric chemical sensors in air and in liquid are known applications of this principle. To measure the crystal resonant frequency that it is directly related to the properties of the load, the crystal is most frequently inserted as the frequency-controlling element of a feedback oscillator circuit. Ideally, the circuit oscillation frequency should be exactly equal to the sensor resonant frequency under every load condition. In practice, this happens only for moderate loads with negligible losses, such as for thin and rigid films in in-air operation. On the contrary, under heavy loading such as encountered with thick viscoelastic coating films or in-liquid operation, significant losses are introduced distorting the sensor impedance around resonance [1, 2]. In such circumstances, a conventional oscillator can cause high inaccuracies determined by the combination of its phase response and that of the sensor. The latter, in turn, is a function of the load and therefore cannot be corrected for as a systematic effect. In the worst case, the circuit eventually stops oscillating and the sensor operating range is limited. Impedance spectral analysis can circumvent this problem [2, 3], but it tends to be costly and more suitable to laboratory environment than sensor applications. In this Letter, we propose a circuit configuration which retains the simplicity and ready applicability of oscillators, while at the same time overcoming the above limitations.

Loaded quartz-resonator sensor: The lumped-element model of Fig. 1*a* approximates the electrical impedance of a loaded quartz sensor around the resonant frequency relative to a given mode number [1, 4, 5]. The crystal is represented by the electrical capacitance C_0 and the equivalent motional elements C_1, L_1 and R_1. The surface load is represented by its equivalent impedance Z_{eq}^L. The added capacitance C_p accounts for the connections, packaging

and, where applicable, the dielectric influence of the load. The series resonant frequency $f_s \approx 1/(2\pi\sqrt{L_T C_T})$, with L_T and C_T being the total motional inductance and capacitance, is typically the quantity to be measured, as it is related to the energy-storage properties of the load and is not affected by the parasitic capacitance C_P. The dissipative effects accounted in the total resistance R_T influence the quality factor $Q = 2\pi f_s L_T/R_T \approx 1/2\pi f_s C_T R_T$. The sensor admittance phase at f_s is given by $\Phi(f_s) = \arctan[2\pi f_s R_1 C_0^*] = \arctan[C_0^*/QC_1]$, where $C_0^* = C_0 + C_P$.

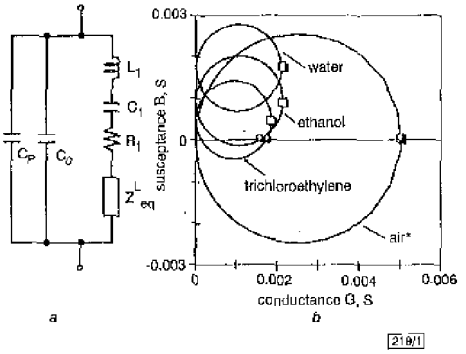

Fig. 1 *Lumped equivalent circuit of loaded quartz-crystal-resonator sensor and admittance circles of 10MHz quartz crystal in air and immersed in different liquids*

a Lumped-element equivalent circuit of loaded quartz-crystal-resonator sensor
b Admittance circles of 10MHz quartz crystal in air and immersed in different liquids
$\divideontimes$ = tenfold downscaling in plot
□ f_s
○ f_r

For a simple mass load, i.e. purely gravimetric regime, Z_{eq}^L is inductive, $R_T = R_1$ and $C_T = C_1$. Therefore, due to the high intrinsic Q of quartz, $\Phi(f_s) \approx 0$ and $\Phi(f)$ is very steep around f_s. By contrast, heavy loads increase losses, leading to $R_T > R_1$ and lowering Q. Additionally, especially for in-liquid operation, C_0^* may also significantly increase due to a rise in C_P. The typical situation comprising both effects is shown in Fig. 1*b*, showing the measured admittance circles for a 10MHz quartz in air and in different liquids. The circle diameters are proportional to Q, while the centre ordinates equal $2\pi f_s C_0^*$. As $\Phi(f_s) \neq 0$ and f_s significantly differs from the zero-phase frequency f_r, f_s can no longer be associated with any constant and load-independent value of the sensor phase.

Oscillator design: The proposed design is based on forcing the sensor phase at f_s to always be zero irrespective of the load, and then track f_s accurately using a phase locked loop oscillator which constantly maintains $\Phi = 0$ across the sensor. The first condition can be obtained by cancelling the overall parallel capacitance C_0^* of the quartz sensor. In fact, if C_0^* is made zero, the phase $\Phi(f_s)$ vanishes for any amount of losses which solely determines the phase slope. This is equivalent to displacing the admittance circles of Fig. 1*b* downward until the centre ordinate is zero. Then, irrespective of the value of Q, hence of the loading, the series resonant frequency f_s and the zero-phase frequency f_r coincide as for an unperturbed crystal.

A block diagram of the oscillator circuit is shown in Fig. 2. The cancellation of the sensor parallel capacitance is accomplished by the active stage built around the high-frequency operational amplifiers *A*1 and *A*2. *A*1 and *R* effectively form an admittance-to-voltage converter, while *A*2, C_c, R_{c1} and R_{c2} generate an equivalent negative capacitance $C_e = -CR_{c2}/R_{c1}$ in parallel with the quartz crystal. If C_c is tuned to equal C_0^*, the total capacitance across the quartz becomes zero and $\Phi(f_s) = 0$. In the same way, the parallel resonant frequency $f_p = 1/(2\pi\sqrt{[L_T C_0^* C_T/(C_0^* + C_T)]})$ equals infinity and the frequency response function V_o/V_i of the active quartz stage, apart from a sign inversion, is reduced to that of a pure series resonant circuit with losses. Even if C_c and C_0^* are not exactly equal, the method is still expected to be effective as long as f_p is pushed to a sufficiently high frequency to allow a complete 180° rotation of the sensor phase around f_s. Assuming a linear asymptotic approximation for the phase, the minimum required frequency spacing is $(f_p - f_s)/f_s = \pi/2Q$.

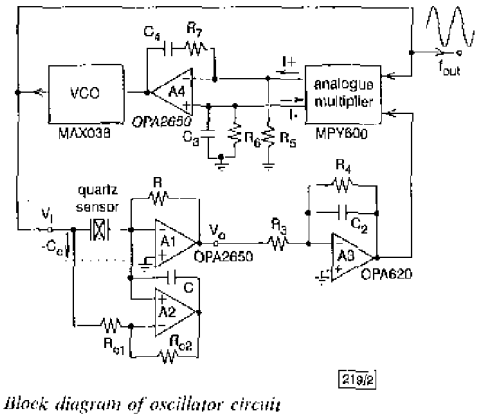

Fig. 2 *Block diagram of oscillator circuit*

The phase locked loop for constantly tracking f_s is made using a sinusoidal voltage-controlled-oscillator (VCO), a 90°-phase shifter (built around *A*3), an analogue multiplier, and a loop filter with a pole in the origin (built around *A*4) to maintain a zero static phase error. The following initial procedure is used to adjust the circuit for a virtually zero error. If the approximate value of C_0^* is known, C is chosen and R_{c2} is trimmed in order to obtain the required value of C_c. Under unknown loading conditions, C_c should be gradually increased starting from approximately C_0 until the oscillation frequency f_{out} asymptotically approaches a constant value, which is expected to equal f_s.

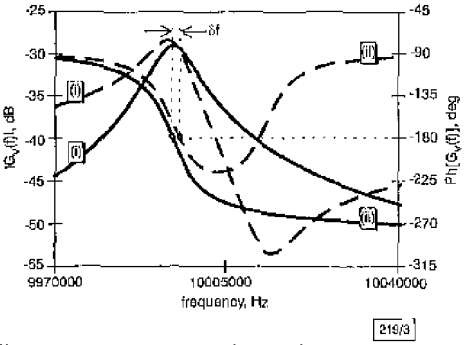

Fig. 3 *Frequency response magnitude and phase of capacitance-cancellation circuit connected to 10MHz crystal immersed in trichloroethylene with and without compensation inserted*

(i) frequency response magnitude
(ii) phase
– – – – without compensation
——— with compensation

Table 1: Experimental results for a 10MHz crystal immersed in trichloroethylene and the oscillator connected to it without (NC) and with (C) the parallel capacitance compensation

Parameter	NC	C
crystal f_s [Hz]	9994040 ± 10	
crystal f_r [Hz]	9995280 ± 10	
f_{out} [Hz]	9995450 ± 5	9994150 ± 3
$f_{out} - f_s$ [Hz]	1410 ± 11	110 ± 10
σ_f^* [Hz]	0.9	0.6

* = 100 samples at measuring time = 0.2s

Results: The actively-compensated stage was connected to a 10MHz quartz fully immersed in trichloroethylene and first tested separately from the oscillator by measuring its frequency response function $G_V = V_o/V_i$. The following impedance parameters were measured for the loaded quartz: L_T = 9.18mH, C_T = 27.65fF, R_T = 550Ω, and C_0^* = 7.68pF. The adopted component values were

$R = 27\Omega$, $R_{c1} = R_{c2} = 1\,k\Omega$ and $C = 6.8\,pF$. Fig. 3 compares the frequency responses obtained with and without the capacitance compensation, showing that the cancellation of the effect of C_0' is successful over the frequency region of interest. The whole oscillator circuit was then tested with the quartz in trichloroethylene. The frequency error caused by the oscillator can be defined as $f_{out} - f_s$, where f_{out} is the circuit oscillation frequency and f_s is the series resonance derived by the impedance measurements previously made on the quartz alone. As shown in Table 1, the non-compensated frequency error was 1410Hz, equal to ~25% of the shift from the unloaded condition. In the compensated case, the frequency accuracy successfully improves by more than an order of magnitude. The residual error is due to minor non-idealities in the overall circuit phase response. Assuming a perfectly ideal phase response, the oscillator frequency error in the absence of compensation corresponds to the frequency difference δ_f shown in Fig. 3. Table 1 also reports a measured reduction in the frequency jitter σ_f for the compensated oscillator that can be ascribed to the increase in the phase slope observable in Fig. 3 compared the uncompensated case. The correct circuit operation was also verified with the quartz immersed both in ethanol and in water. In the latter case, as shown in Fig. 1*b*, the high acoustic and dielectric loading prevent the sensor phase from reaching the zero crossing, which in turn prevented the circuit from oscillating without compensation. Despite this, the compensated configuration succeeded in keeping the crystal resonating. The oscillator can be improved by automating the compensating capacitance tuning procedure, and by including a rectifier and an automatic-gain-control stage to also measure the degree of damping of the sensor.

Acknowledgments: The contribution of A. Colpani and R. Rolfi in the laboratory activity is greatly acknowledged.

16 December 1999
Electronics Letters Online No: 20000493
DOI: 10.1049/el:20000493

V. Ferrari, D. Marioli and A. Taroni (*Dipartimento di Elettronica per l'Automazione, Facoltà di Ingegneria, Università di Brescia, Via Branze 38, 25123 Brescia, Italy*)

References

1 AUGE, J., HAUPTMANN, P., HIELBAUM, F., and RÖSLER, S.: 'Quartz crystal microbalance sensor in liquids', *Sens. Actuators B*, 1994, **18–19**, pp. 518–522

2 MARTIN, S.J., EDWARDS GRENSTAFF, V., and FRYE, G.C.: 'Characterization of quartz crystal microbalance with simultaneous mass and liquid loading', *Anal. Chem.*, 1991, **63**, pp. 2272–2281

3 HICHELBAUM, F., BORNGRÄBER, R., SCHRÖDER, J., LUCKLUM, R., and HAUTMANN, P.: 'Interface circuits for quartz-crystal-microbalance sensors', *Rev. Sci. Instrum.*, 1999, **70**, (5) pp. 2537–2545

4 CERNOSEK, R.W., MARTIN, S.J., HILLMAN, A.R., and BANDEY, : 'Comparison of lumped-element and transmission-line models for thickness-shear-mode quartz resonator sensors', *IEEE Trans.*, 1998, **4**, (UFFC 45), pp. 1399–1407

5 FILIATRE, C., BARDICHE, G., and VALENTIN, M.: 'Transmission-line model for immersed quartz-crystal sensors', *Sens. Actuators A*, 1994, **44**, pp. 137–144

Capacity of various exponential bidirectional associative memories

Tae-Dok Eom, Choon-Young Lee and Ju-Jang Lee

The capacities of various exponential bidirectional associative memories (eBAMs) are derived and compared.

Introduction: Bidirectional associative memory has been widely used to solve classification problems such as pattern recognition \cite{BAM}, data compression [1], etc. Since Jeng *et al.* [2] proposed eBAM, which has a high storage capacity and error-correction capability as well as being simple to implement, a great deal of research has gone into further improving its performance. The modified eBAM (MeBAM) proposed by Wang and Lee [3] introduced intraconnections in the eBAM to remove the additional encoding problem and continuity assumption. Chen *et al.* [4] pointed out that there was hardly any improvement in the storage capacity and error-correction capability of the MeBAM compared with that of the eBAM, and proposed an improved eBAM (IeBAM). Apart from proving that Wang's capacity result [1], in which the probability distribution does not total one, is erroneous, these eBAM models do not involve rigorous analysis. In this Letter, we use computer simulations to show the improved performance of those models.

In the following capacity analysis, we assume there are p stored pattern pairs $\{(\mathbf{x}^i, \mathbf{y}^i)\}_{i=1}^{p}$, where $\mathbf{x}^i \in \{-1, 1\}^n$ and $\mathbf{y}^i \in \{-1, 1\}^m$. Each bipolar element of the patterns is randomly generated with equal probability. Further, we assume $n = m$ to show the capacity difference of the various eBAM models.

eBAM: The bidirectional recall process of the eBAM in one cycle is

$$\mathbf{y} = f(\mathbf{x}) = \mathrm{sgn}\left(\sum_{i=1}^{p} \mathbf{y}^i b^{\mathbf{x}^{iT}\mathbf{x}}\right) \tag{1}$$

$$\mathbf{x}' = g(\mathbf{y}) = \mathrm{sgn}\left(\sum_{i=1}^{p} \mathbf{x}^i b^{\mathbf{y}^{iT}\mathbf{y}}\right) \tag{2}$$

where $b > 1$ and $\mathrm{sgn}(u) = 1$ if $u \geq 0$ and $\mathrm{sgn}(u) = -1$ otherwise.

Considering the forward association eqn. 1, $y_k^h f_k(\mathbf{x})$ should be greater than zero for $\forall h$ and $\forall k$ given an attraction radius r, i.e. the Hamming distance between $\mathbf{x}$ and $\mathbf{x}^h$, $d_H(\mathbf{x}, \mathbf{x}^h)$, is r. According to eqn. 1

$$y_k^h y_k = \mathrm{sgn}\left(b^{n-2r} + \sum_{i \neq h} y_k^h y_k^i b^{\mathbf{x}^{iT}\mathbf{x}}\right) > 0 \tag{3}$$

We define $v^i = y_k^h y_k^i b^{\mathbf{x}^{iT}\mathbf{x}}$, which gives

$$\Pr(v^i = +b^{n-2s}) = \Pr(y_k^h y_k^i = 1) \cdot \Pr(d_H(\mathbf{x}^i, \mathbf{x}) = s) = \frac{1}{2} \cdot \left(\frac{1}{2}\right)^s \left(\frac{1}{2}\right)^{n-s} C_s^n = \left(\frac{1}{2}\right)^{n+1} C_s^n$$

$$\Pr(v^i = -b^{n-2s}) = \left(\frac{1}{2}\right)^{n+1} C_s^n$$

Using this symmetric probability distribution, we can easily obtain $E[v^i] = 0$ and

$$E[v^{i2}] = \sum_{s=0}^{n} b^{2n-4s} 2\left(\frac{1}{2}\right)^{n+1} C_s^n \tag{4}$$

$$= \left(\frac{b^2}{2}\right)^n \sum_{s=0}^{n} b^{-4s} 1^{n-s} C_s^n = \left(\frac{b^2}{2}\right)^n (1 + b^{-4})^n \tag{5}$$

Since the overall noise v is the sum of $(p-1)$ identical random variables, v^is, $\sigma_v^2 = (p-1)E[v^{i2}]$. Henceforth, the error of the recall process occurs when $v < -b^{n-2r}$ in eqn. 3. Based on the central limit theorem which holds as $n, p \to \infty$, the bit error probability P_e is as follows:

$$P_e = \Pr(v < -b^{n-2r}) = Q\left(\frac{b^{n-2r}}{\sigma_v}\right) \tag{6}$$

where $Q(u) = 1/\sqrt{(2\pi)}\int_u^\infty e^{-t^2/2}\,dt$.

We now analyse the capacity. For numbers of noisy patterns to be directly attracted to the stored patterns, the expected number of error bits after a one-step update has to be less than one, i.e. the condition $nQ(U) < 1$ has to be satisfied, where the expression for U is seen in eqn. 6. Using the approximation $Q(U) = 1/\sqrt{(2\pi)}U^{-1}e^{-U^2/2}$, we can obtain the stronger condition $-U^2/2 + \log n < 0$, taking the most dominant terms into account. Replacing this inequality condition by an equality, we obtain the critical condition for the capacity

$$p_{eBAM}^c \simeq \frac{1}{2\log n} \cdot \frac{2^n b^{-4r}}{(1 + b^{-4})^n} \tag{7}$$